RSC Advances

PAPER

View Article Online
View Journal | View Issue

Cite this: *RSC Adv.*, 2024, **14**, 29624

Enhanced properties of TEMPO-oxidized bacterial cellulose films *via* eco-friendly non-pressurized hot water vapor treatment for sustainable and smart food packaging

Dieter Rahmadiawan,[ab] Hairul Abral,*[cd] Muhammad Adlan Azka,[e] S. M. Sapuan,[e] Ratna Isnanita Admi,[f] Shih-Chen Shi,[a] Rahadian Zainul,[g] Azril,[h] Ahmad Zikri[i] and Melbi Mahardika[j]

Received 22nd August 2024
Accepted 9th September 2024

DOI: 10.1039/d4ra06099g

rsc.li/rsc-advances

Developing a simple and environmentally friendly method to vary the physical, mechanical, and thermal properties of cellulose films is of great importance. This study aimed to characterize 2,2,6,6-tetramethylpiperidinyl-1-oxyl (TEMPO)-oxidized bacterial cellulose (BC) films prepared using non-pressurized hot water vapor (NPHWV) method. A wet BC-pellicle that had been oxidized with TEMPO was treated with NPHWV for 60, 120, and 240 minutes, respectively. As a control, a TEMPO-oxidized BC (TOBC) film without NPHWV was prepared. The results show that the longer NPHWV duration of the TOBC film increased the tensile and thermal properties. This film became more hydrophobic and showed lower moisture absorption, thermal conductivity and organic solvent uptake, more crystalline structure, and higher fiber density after NPHWV treatment. The acquired results provide a simple, inexpensive, and ecologically friendly method for varying TOBC film properties.

1. Introduction

In recent years, advanced materials have garnered significant attention due to their remarkable mechanical, electrical, and thermal properties.[1,2] However, despite these promising attributes, the widespread use of such materials faces several limitations. Their production processes can be energy-intensive, costly, and often involve hazardous chemicals. In light of these drawbacks, the focus has increasingly shifted toward more sustainable alternatives derived from natural resources.[3–5] Among these natural resources, cellulose stands out due to its abundance, renewability, and biodegradability.[6,7] Cellulose, a fundamental component of the cell walls in green plants, algae, and some bacteria, plays a crucial role in maintaining structural integrity. Its unique properties, such as high tensile strength, rigidity, biodegradability, low cost, and non-toxic nature, make it a highly versatile material.[7,8] Cellulose can be engineered into various forms, including ultrathin films (below 10 nm), which offer promising potential for advanced applications like sensors, coatings, and biointerfaces due to their high surface area and tunable properties.[9] Due to these properties, cellulose has garnered substantial interest, particularly in sustainable and environmentally friendly technologies.[10,11] As a biodegradable and renewable resource, it offers a promising alternative to synthetic materials in various applications, ranging from packaging to textiles, and even in the development of biomedical materials.[12]

Bacterial cellulose (BC) attracts considerable interest as another major source of cellulose.[13] BC is a plentifully produced kind of natural cellulose that is synthesised by *Acetobacter xylinum*. It occurs in the form of BC pellicle, also known as *nata de coco*.[14,15] Nata de coco may be consumed straight due to its high purity. It contains no contaminants, such as hemicellulose and lignin in wood fibres.[16] BC pellicle is a hydrogel with a high water content of over 90%.[17] The highly crystalline BC nanofibers cross-

[a]*Department of Mechanical Engineering, National Cheng Kung University (NCKU), Tainan, Taiwan*
[b]*Department of Mechanical Engineering, Universitas Negeri Padang, 25173 Padang, Sumatera Barat, Indonesia*
[c]*Department of Mechanical Engineering, Andalas University, 25163 Padang, Sumatera Barat, Indonesia. E-mail: habral@yahoo.com*
[d]*Laboratory of Nanoscience and Technology, Department of Mechanical Engineering, Andalas University, 25163 Padang, Sumatera Barat, Indonesia*
[e]*Advanced Engineering Materials and Composites Research Centre, Department of Mechanical and Manufacturing Engineering, Universiti Putra Malaysia, 43400 UPM Serdang, Selangor, Malaysia*
[f]*Laboratory of High-Temperature Coating, Research Center for Physics Indonesian Institute of Sciences (LIPI) Serpong, Indonesia*
[g]*Department of Chemistry, Faculty of Mathematics and Natural Science, Universitas Negeri Padang, West Sumatera 25171, Indonesia*
[h]*Department of Biomedical Engineering, National Cheng Kung University, Tainan, Taiwan*
[i]*Department of Mechanical Engineering, Faculty of Engineering, Bursa Uludag University, Bursa 16850, Turkey*
[j]*Research Center for Biomass and Bioproducts, National Research and Innovation Agency (BRIN), Cibinong, Indonesia*

link to produce a unique 3D network structure with significant porosity.[18] Dry BC pellicle films may have a tensile strength greater than 200 MPa due to their unique structure and excellent purity.[19] As a result, BC is a versatile material that is widely used in various applications such as functional paper, biological materials, electronic devices, and lubricants additive.[20] However, BC is difficult to apply to flexible devices due to its lack of flowability, which is a key property of polymer processability.[21] Therefore, this limits BC's possibilities for more advanced applications.

Some previous works have reported using the TEMPO method to increase the properties of the BC film.[22,23] This process weakens the hydrogen bonds in the BC polymer chain.[21,24] For example, Huang *et al.*[25] used the TEMPO system on BC pellicles to modify the physical and mechanical properties of separation membranes for batteries. This study found that the tensile strength and toughness of the TOBC film increases with increasing TEMPO concentration. This approach, nevertheless, has the drawback of involving complex procedures and the use of many radical-generating chemicals.[26] In contrast, the characteristics of cellulose-based films may also be modified using simple, ecologically friendly processes.[27] For instance, Suzuki *et al.*[28] used steam detonation at various pressures and durations to modify the characteristics of cellulose nanofibers generated from Japanese cedar wood. The steaming technique produces hot vapor with high pressure and temperature, making it a chemical-free process. Steam energy may enhance the mobility and adhesion of polymer chains *via* mechanical forces,[29–31] they can also result in reduced crystallinity. Previous studies have shown that high-pressure steam treatments can decrease crystallinity, likely due to the disruption of the ordered regions of cellulose caused by the high pressure.[32] In this work, we explore the effects of non-pressurized hot water vapor (NPHWV) treatment on TOBC films, as there has been limited research on how non-pressurized steam impacts TOBC films. Therefore, the objective of the present work was to evaluate the properties of TOBC films without and with NPHWV for various durations. The benefit of this study is to increase a better understanding of the effect of NPHWV treatment on the characteristics of TOBC films. The properties of the film measured were tensile and thermal properties, organic solvent uptake, water contact angle, moisture absorption, *etc.* Meanwhile, X-ray diffraction (XRD), Fourier transform infrared spectroscopy (FTIR), FESEM photograph of the surface was used to identify chemical features, interactions of all functional groups, and defects in the film. By systematically investigating these properties, this study provides valuable insights into the potential of NPHWV treatment as a simple, sustainable, and effective method for enhancing the performance of TOBC films. This enhancement broadens their applicability in various high-performance, sustainable, and smart food packaging applications.

2. Materials and methods

2.1 Materials

The *nata de coco* pellicle (30 × 20 × 0.7 cm) was obtained from the home industry in Bekasi, Indonesia. The *nata de coco* pellicle was purified using distilled water and analytical-grade sodium hydroxide (NaOH) from Andeska Laboratory to remove the residual on the *nata de coco* pellicle before use. TEMPO, sodium bromide (NaBr), and *n*-butanol (purity ≥99.5%) were purchased from Sigma-Aldrich. Sodium hypochlorite (NaClO) was supplied by Citra Sari Kimia. Acetone was purchased from Dwipraga Chemical.

2.2 Methods

2.2.1 Production of BC pellicle. Pure coconut water was filtered to filter dirt on the coconut water. Filtered coconut water was boiled at 75 °C and mixed with 1.5% (wt/v) sugar, 0.25% (wt/v) ammonium sulfate. The mixture was adjusted to pH 4 using 0.35% (v/v) glacial acetic acid. Thereafter the mixture was boiled at 95 °C for 15 minutes to kill pathogenic bacteria. The mixture was poured into the molding and covered with sterile paper for 24 h. 10% (v/v) *Acetobacter xylinum* was mixed into the mixture and covered again with sterile paper and fermented for 14 days to form BC pellicle. Cellulose content in the BC pellicle is above 92%, as reported by Vahana Scientific Lab in Padang, Indonesia.

2.2.2 Preparation of TOBC pellicle. The BC pellicle (30 × 20 × 0.7 cm) was cleaned with distilled water and soaked in 10% NaOH solution for 48 h and rinsed with distilled water until pH 7, then cut into 10 × 15 cm. BC pellicle was clamped to reduce water content and stored with acetone. 300 ml of distilled water is mixed with 0.016 g of TEMPO, 0.1 g of NaBr and stirred using a hot plate magnetic stirrer at 650 rpm for 5 minutes. Then BC pellicle is added to the TEMPO solution and stirred for 5 minutes using a hot plate magnetic stirrer. Then add NaClO (12%) 8 ml and boil at 70 °C for 6 h and stir at 650 rpm with a hot plate magnetic stirrer. Let stand TOBC pellicle for 12 h and then rinse and soak with distilled water until pH 7.

2.2.3 Preparation of TOBC films without and with non-pressurized steam treatment. Wet TOBC pellicle was steamed using a steamer (Smart Keuken Gen 2, 500 W, China). The desired amount of distilled water was poured into a stainless-steel pot, thereafter steam pot was put above the stainless steel pot in the steamer and the sheet of *nata de coco* was put in the steam pot and steamed with time variations of 0 h, 1 h, 2 h, and 4 h (TNS, TS1, TS2, TS4). The TNS, TS1, TS2, TS4 were dried in the oven at 100 °C for 6 h.

2.3 Characterization

2.3.1 Field emission scanning electron microscopy (FESEM) and physicochemical properties. A field-emission scanning electron microscope FEI Nova NanoSEM 230 (FEI, Brno-Černovice, Czech Republic) was used with 5 kV at 1 000 00x magnification to observe the surface morphology of the sample. Before the samples were observed, the samples were coated with carbon followed by gold for two minutes using an argon plasma metallizer (sputter coater K575X) (Edwards Limited, Crawley, United Kingdom) to reduce the electron charge. Porosity percentage was determined by following eqn (1)

$$\text{Porosity } (\%) = \frac{(w_i - w_o)}{(\rho_b \times V_0)} \times 100 \quad (1)$$

w_i and w_o are is the weight after absorption and initial sample weight, ρ_b and V_0 are the density of *n*-butanol and volume sample. Porosity percentage was measured by immersing *n*-butanol for 1 h, and *n*-butanol liquid on the sample surface was cleaned use filter paper before weighting.

The thickness of the films were observed with an optical microscope (Olympus Stereo Microscope SZX10). Thermal conductivity was measured using a Quick Thermal Conductivity Meter (QTM-500) manufactured by Kyoto Electronics Manufacturing CO. Ltd Japan. The measurement used the hot wire method (I^2 0.250 A^2) that uses Probe PD-11 (polymer/composite probe). The measurements begin by placing the sample in the probe box and then placing the probe on the sample surface. The heating wire will supply heat to the sample, and the thermocouple will detect the heat flow rate. The required sample size for measurement is 100 mm × 50 mm and conditioned at room temperature (22–24 °C) and relative humidity (60–70%). The thermal conductivity of the samples was measured using thin film measurement testing parameters with reference material (polyethylene foam, silicone rubber, and quartz glass). The samples were dipped in *n*-butanol on a Petri dish and waited for 30 minutes to measure the organic solvent uptake.

The immersed electrolyte was measured using a digital vernier caliper to obtain the height of immersed electrolyte. The sample dimension was 10 mm × 45 mm and conditioned using a Universal Oven Memmert UN-55 at 50 °C for 12 h.

Organic solvent uptake was measured by absorbing *n*-butanol for 1 h. The extra *n*-butanol liquid on the sample surface was wiped using filter paper before weighting. Organic solvent uptake percentage was determined by following eqn (2)

$$\text{Organic solvent uptake } (\%) = \frac{(w_i - w_o)}{w_o} \times 100 \quad (2)$$

w_i is the weight after absorption w_o initial sample weight.

X-ray diffraction testing was carried out using PANalytical Xpert PRO at 25 °C, 40 kV, and 30 mA. The samples were scanned from $2\theta = 10°$ to 30°. The percentage of CrI was measured using Segal equation method eqn (3):

$$\text{CrI } (\%) = \frac{(I_{200} - I_{am})}{I_{200}} \times 100 \quad (3)$$

where I_{200} is the 200 peak ($2\theta = 22.79°$) and I_{am} is the minimum intensity between the 101 and 200 peaks ($2\theta = 20°$).

2.3.2 FTIR. Fourier transform infrared (FTIR) spectra characterization was collected using a Shimadzu IRTracer-100 FT-IR spectrometer. The sample was scanned at wavenumber from 4500–400 cm^{-1}.

2.3.3 Moisture absorption. Moisture absorption was measured using a closed container containing a saturated non-iodized salt solution with relative humidity (75%) at room temperature for 8 h. The samples were dried using a Universal Oven Memmert UN-55 at 50 °C for 12 h. Dried samples were weighted to determine the initial weight of the samples. Measurement begins by taking out samples and weighing for every 30 min using a Kenko Precision Balance. Moisture absorption percentage was determined by following eqn (4)

$$\text{Moisture absorption } (\%) = \frac{(w_i - w_o)}{w_o} \times 100 \quad (4)$$

w_i is the weight after absorption w_o initial sample weight.

2.3.4 Contact angle. Contact angle was measured using Theta Lite by attaching samples to the equipment and dropping water on the sample surface, then measured and photographed immediately. The contact angle samples were measured between the surface and the tangent water drops (°) and measured in first 10 s.

2.3.5 Tensile properties. The tensile properties of the sample were obtained using a Universal Testing Machine (UTM) (AGS-X series 5 kN, Shimadzu, Japan) at a 5 mm min^{-1} tensile test speed. The sample dimension used the ASTM D638-type V standard. The tests were repeated five times for each sample.

2.3.6 Thermogravimetric Analysis (TGA) and derivative (DTG). Thermogravimetric Analysis (TGA) and Derivative (DTG) were measured using TGA 5500 (TA Instruments CO., USA). The measurement was carried out from room temperature until 600 °C with 20 °C min^{-1} heating rate and 50 ml min^{-1} nitrogen flow rate.

2.3.7 Statistic analysis. The experimental data was analyzed using IBM SPSS Statistics 25.0 (IBM Corporation, Chicago, USA). To determine the significance of the influence of each treatment on the film properties, a one-way analysis of variance (ANOVA) and p-test were conducted. The multiple range test of Duncan was conducted with a confidence level of 95% ($p \leq 0.05$).

3. Results and discussions

3.1 Morphology and physicochemical properties of the films

Fig. 1 depicts the FESEM morphology of film surfaces. Non-steamed sample (Fig. 1a) has a greater porosity fraction than steamed samples (Fig. 1b–d). The high pore volume may be due to the weakening of fiber bonds induced by TEMPO treatment.[21,25] After being vaporized, the density of pores decreased and fibers became denser, thus resulting in formation of less cavity. This result is because the increased temperature increases the activation energy of the polymer chains, allowing them to move and resulting in a smaller pore diameter. Hence, the steamed film had more compact structures and a higher fiber density fraction than the non-steamed ones. The NPHWV treatment increases the moisture content within the cellulose structure. This increased mobility of the cellulose chains leads to a reorganization of hydrogen bonds. Upon cooling, new hydrogen bonds may form between the cellulose molecules, leading to a denser structure as the water evaporates. The heat and moisture together can promote a closer packing of the cellulose chains, reducing porosity.[33] This result aligns with the measurements displayed in Fig. 2, which show the steamed films' diminishing water-absorption capacity over time. It also consistent with the physicochemical properties listed in Table 1. It can be seen that the film thickness decreases with longer

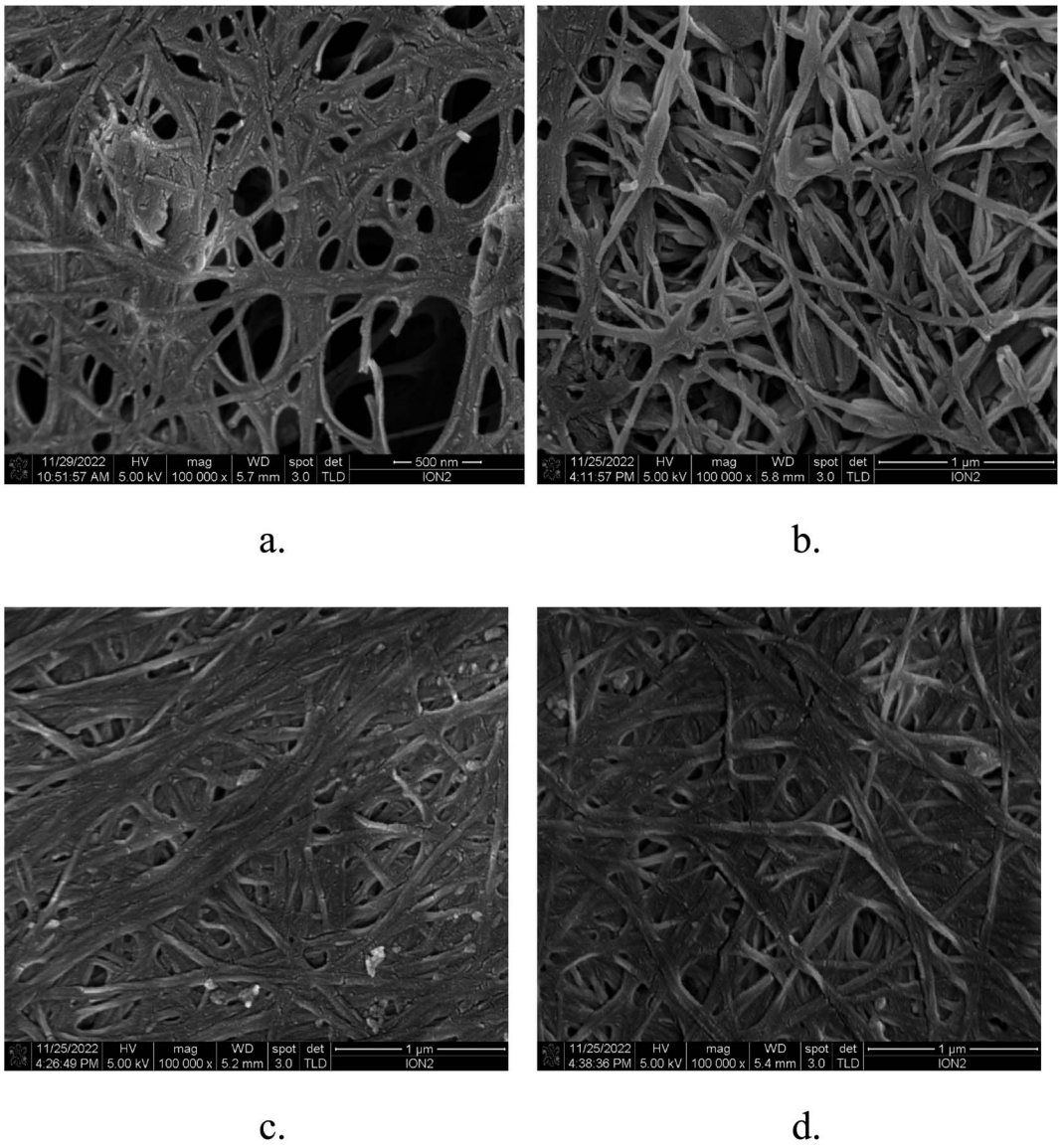

Fig. 1 FESEM morphology of the film surfaces of TNS (a), TS1 (b), TS2 (c), and TS4 (d).

steaming durations. Compared to TNS, the thickness of the TS4 film was reduced by 19%. Correspondingly, thermal conductivity also decreases with increasing steam treatment duration. The untreated sample, TNS, has the highest thermal conductivity of 0.0832 W (m K)$^{-1}$, while the sample treated for 4 h, TS4, has the lowest at 0.0537 W (m K)$^{-1}$. This might be because of the structure of compact BC. This compaction could blocking free path of the air and voids through which heat can easily transfer, thereby reducing the material's overall thermal conductivity.[34] On the other hand, while increased crystallinity is typically associated with higher thermal conductivity due to more ordered molecular chains, in this case, the increase in crystallinity coupled with a decrease in porosity suggests a tighter packing of the cellulose chains. This tighter packing might reduce the mobility of the molecular chains, limiting their ability to transfer heat. The photo images of BC and TOBC films can be seen in our previous work.[35]

3.2 FTIR spectra

Fig. 2 shows the FTIR spectra for non-TEMPO BC film (NTNS) and TEMPO-oxidized BC-pellicle films without (TNS) and with steam treatment (TS1, TS2, and TS4). This pattern agrees with previous works.[36,37] All patterns in Fig. 2 are broadly similar, which indicates that the treatment did not induce undesirable chemical modification. However, processing through TEMPO oxidation and the various steam duration of film shifted the peak area and wavenumbers and intensities of the spectrum peaks. The shifting may be attributed to the hydrogen bonding interactions.[36] This structural change is consistent with the XRD pattern shift (Fig. 3). The wavenumbers at around 1645 cm^{-1} corresponds to O–H bending of the absorbed water.[38,39] This peak position, however, decreased after being steamed. For example, the wavenumber for TS1, TS2, and TS4 film was 1610, 1606, and 1602 cm^{-1}, respectively, lower than TNS film (1616 cm^{-1}). This phenomenon may be due to increased

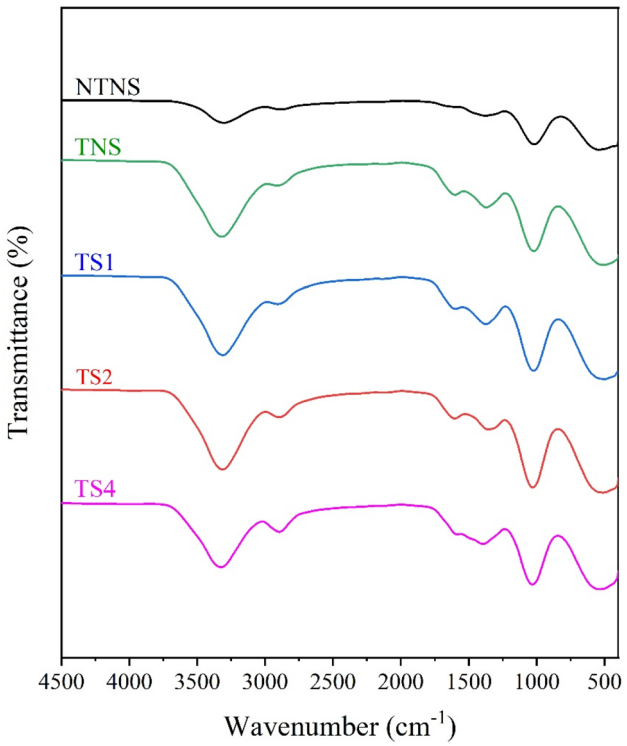

Fig. 2 The FTIR spectrum of films with different treatments.

number of hydrogen bonds formed between chains (intermolecular hydrogen bonding) or within the same chain (intramolecular hydrogen bonding).[40] A similar phenomenon also was observed in higher transmittance (T) value of water bending vibrations after treatment. For example, T value of TS1, TS2, and TS4 film was 78.8%, 81.8%, and 81.2%, respectively (Table 1), higher than TNS film (78.1%). This weak peak intensity of steamed films may correspond to low concentration of free –OH groups available in the polymer chains having a more compact and crystalline cellulose structure.[41,42] In such structures, the hydroxy groups are involved in strong, consistent hydrogen bonding, which is characteristic of well-aligned and orderly cellulose chains. This strong intermolecular hydrogen bonding leads to a more uniform bonding environment for the hydroxy groups, resulting in a sharper and narrower O–H stretching band. Therefore, the presence of a narrow O–H band is generally associated with a high degree of crystallinity, where the cellulose chains are tightly packed and aligned in a regular, ordered pattern, consistent with the data presented in Table 1. A similar finding agrees with previous work.[42,43]

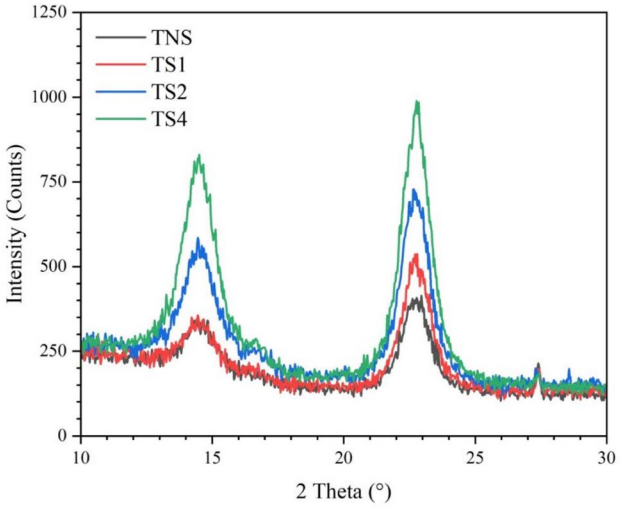

Fig. 3 XRD curves for all samples without and with NPHWV for the various duration.

3.3 X-ray diffraction

Fig. 3 displays the X-ray diffraction curves of the membranes without and with steam treatment at different steaming time periods (1, 2, and 4 h). Apparently, all films present similar X-ray diffraction patterns with two main peaks. These position peaks as reported in Table 1 were located at about 14.5° and 22.8° in 2θ associated with the crystallographic planes of (1–10) and (200) crystal structure of cellulose Iα, respectively.[44] The height of the peaks corresponds to the crystallinity index (CrI) of the cellulose-based film.[45,46] Height of these intensity peaks increases with longer steaming periods corresponding to more reordered crystal structures resulting in an increase in crystal fraction.[47,48] Film without steam treatment (TNS) shows a crystallinity index (CrI) of about ~68.1% (Table 1). Furthermore, ongoing from TNS to TS1, TS2, and TS4 films, the height difference between the two peaks at about 14.5° and 22.8° becomes more distinct. The CrI value after steam duration for 1, 2, and 4 h was 72.5% (TS1), 73.8% (TS2), and 81.0% (TS4), respectively. The increased CrI may be due to partial loss of amorphous regions becoming crystalline fractions *via* hydrogen bonding between the neighboring chains.[25] This result agrees with the main peak position shifting toward lower value after steam treatment as a result of restructuring the cellulose chains. The greater activation energy of molecular chains at high temperatures enables them to restructure, resulting in the formation of hydrogen bonds between the polymer chains.[38]

Table 1 Physicochemical properties of the films

Sample	Film thickness (μm)	Thermal conductivity (W (m K)$^{-1}$)	Organic solvent uptake (%)	Porosity (%)	Crystallinity, CrI (%)
TNS	43.7	0.0832	32.2	65.1	68.12
TS1	36.9	0.0766	20.1	40.4	72.47
TS2	36.8	0.0629	13.5	28.4	73.82
TS4	35.4	0.0537	9.4	19.2	81.00

The cellulose chains prefer to organize themselves in such a way that each long molecule is linked to the neighboring chains by hydrogen bonds, resulting in a highly structured crystalline structure.[49] This phenomenon is also consistent to FTIR curve showing lower sharp peak position at wavenumbers of around 1645 cm^{-1} after steam treatment.

3.4 Contact angle

Fig. 4 demonstrates the contact angle (θ) of water on different film surfaces (TNS, TS1, TS2, and TS4) of 9 second duration. θ for TNS, TS1, TS2, and TS4 was 21.47, 35.96, 39.48, and 47.63 respectively. The results reveal that the contact angle increases with increasing film boiling time. This increase in θ value indicates reduced water accessibility, which can be attributed to the increasing compactness and crystallinity of the cellulose structure, resulting in fewer accessible –OH groups. This observation is consistent with the FTIR data, where the TNS sample, with its broader O–H band, indicates more accessible hydroxyl groups compared to the TS4 sample (Fig. 2). Additionally, the reduced water accessibility in the steamed film is attributed to the lower porosity and higher fiber density observed in Fig. 1.

3.5 Water uptake and moisture absorption

Fig. 5a demonstrates the organic solvent uptake of the samples. TNS film shows the best butanol absorption capacity. This membrane wets easily in n-butanol. The height of *n*-butanol level in the non-steam sample is about 10.18 mm. The excellent butanol absorption capacity for this film was due to its highly hydrophilic surface characteristic and abundant –OH group on the membrane.[41,50] This phenomenon agrees with the result in FTIR curve (Fig. 2) showing great area of –OH peak intensity for non-steamed film. Along with the long evaporation of heat increases, the wettability of the film decreases. The wet heights of TS1, TS2 and TS4 films are 4.74, 3.81, and 2.59 mm respectively. This decreased value is consistent with result obtained with moisture absorption measurement (Fig. 5b). In this case, film without steaming exhibits MA of 7.4 ± 0.6% for 480 min in a humid chamber (RH 75%). After steam duration, this MA ability of film decreased significantly. MA value of TS1, TS2, and TS4 was 1.6 ± 0.5%, 1.6 ± 0.5%, and 1.6 ± 0.5%, respectively. This result is probably associated with the increased hydrophobicity of the vapor films due to the reduced porosity density and the increased compactness of the films. Besides, the more hydrophobic nature of the steamed film results from the increasing degree of crosslinking molecules.[23,51] This result is consistent with reducing pore fractions after steam treatment as shown in Fig. 1.

3.6 Electrical properties

Fig. 6a displays closed DC circuits from the connection of NTSN film (white dotted line box), a 3 V light-emitting diode (LED) (solid orange box line in Fig. 6b), and a 9 V battery. After plugging the battery, the LED connected with this non-TEMPO film does not visually glow. This finding corresponds to poor electrical flow in non-TEMPO film. In contrast to Fig. 6d, the LED connected to the TNS sample glows brightly when the battery is plugged. The result demonstrates that film after TEMPO treatment became more conductive. This increased conductivity is due to the TEMPO-oxidation process, which

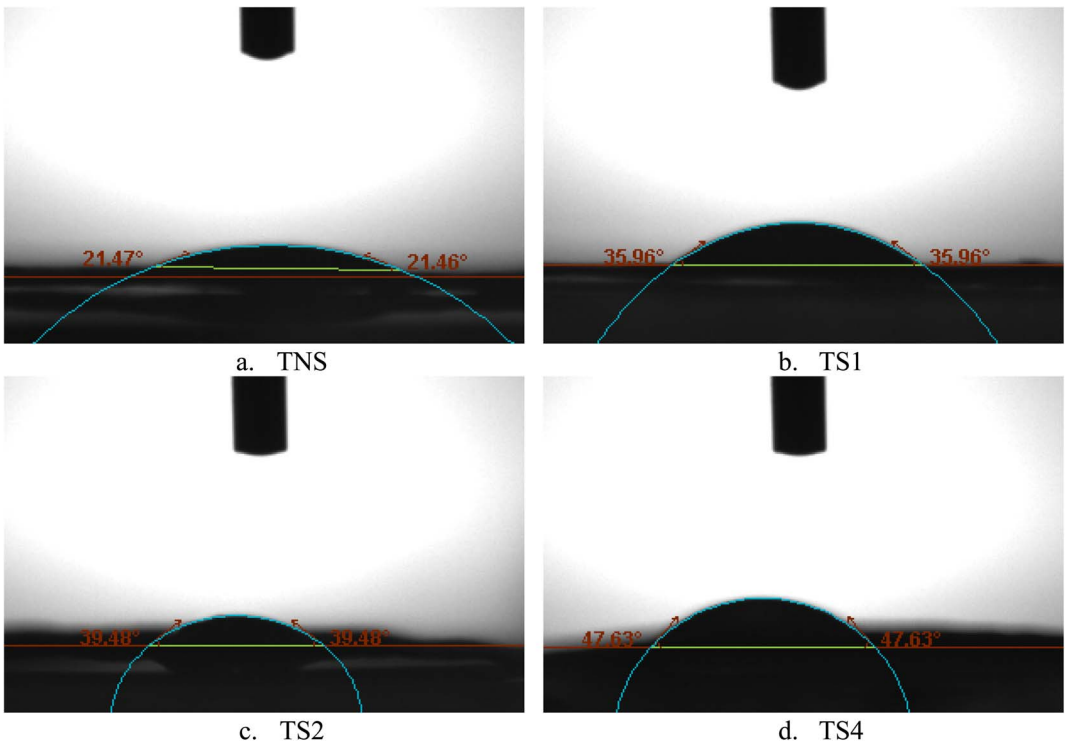

Fig. 4 Images of contact angles (θ) of water on different film surfaces of TNS (a), TS1 (b), TS2 (c), TS4 (d) analysed using image software.

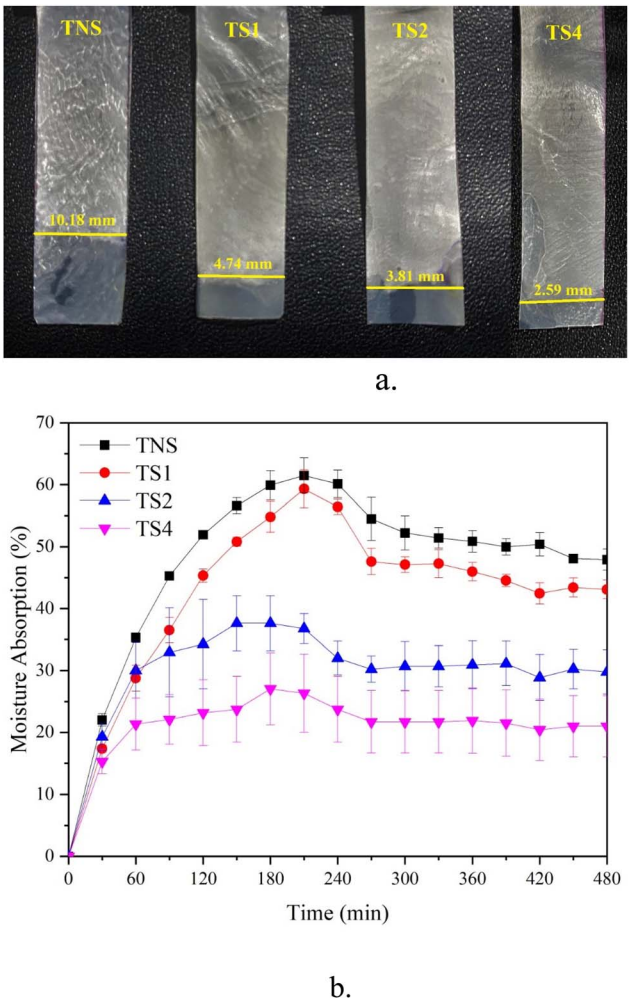

Fig. 5 Effect of steam treatments on organic solvent uptake (a) and moisture absorption performance (b) of films.

introduces carboxylate groups (–COO^-) onto the cellulose chains. These carboxylate groups break inter-fibril hydrogen bonds and introduce anionic sites that can dissociate, increasing ion mobility within the cellulose structure and thereby enhancing electrical conductivity. This mechanism has been demonstrated in recent study, where TEMPO-oxidized cellulose nanofibrils exhibited increased ion mobility and conductivity due to the presence of carboxylate groups and their interaction with moisture.[52] This modification enables the cellulose to inherently conduct electricity. This high conductivity may also correspond to increased hydroxy functional groups of the membrane.[23] A similar finding also was present in previous work.[25] The TEMPO treatment has weakened the hydrogen bonds between the nanofibers resulting in an increased amount of nano/micro-sized porosity as a medium for moving electrons.[53] This phenomenon is consistent with the FESEM results (Fig. 1) which show more porosity for films with TEMPO than without TEMPO. A similar result agrees with previous work.[25] Fig. 6b presents the average electrical resistance and conductivity values for all TOBC films without and with steam. From this figure, the conductivity continued to decrease, and the resistance increased with longer steam durations. The ionic conductivities of TNS, TS1, TS2, and TS4 are 0.35 mS cm^{-1}, 0.26 mS cm^{-1} and 0.24 mS cm^{-1} respectively. This result may correspond to decreasing wettability after steam treatments.[54] This phenomenon was observed in the FTIR curve (Fig. 2), showing that the TS4 film had a lower peak intensity of hydroxy stretching vibration than TNS film. This finding is consistent with decreasing water uptake (Fig. 5a) and moisture absorption properties of films after steam treatment (Fig. 5b).

3.7 Tensile properties

The tensile properties of all treated films are demonstrated in Fig. 7. Each film shows different mechanical behaviors in terms of tensile strength, tensile modulus, toughness, and elongation at break. The TNS sample has the lowest tensile strength and modulus, which is expected as it has not been subjected to any hot water vapor steam treatment. After 1 hour of steam treatment, there is a noticeable increase in both tensile strength and modulus. The steam treatment could be facilitating a better alignment of cellulose chains or promoting cross-linking, thus improving these properties.[55] Extending the steam treatment duration to 2 h results in a further increase in both tensile strength and modulus. However, for the TS4 sample, which underwent 4 h of treatment, there is a reversal of this trend. The tensile strength diminishes slightly in comparison to the TS2 sample, while the tensile modulus continues its upward trajectory. This could be attributable to over-treatment, potentially causing material degradation or inducing excessive cross-linking. Although cross-linking can enhance rigidity, it may also begin to reduce the material's capacity to absorb stress before fracturing.

Conversely, the toughness and elongation at break do not uniformly increase with the treatment duration. Similar with the tensile strength and modulus, the toughness of the films begins to decline following the 4 hour treatment. The enhancement in tensile strength observed with NPHWV treatment is supported by an increase in the crystallinity and reduced porosity of the films, as the steam treatment progresses.[33] In cellulose, regions of high crystallinity are typically much stronger and more rigid due to the dense hydrogen bonding network within the crystal structure. As the steam treatment duration increases, the disruption and realignment of hydrogen bonds during the treatment could lead to a higher degree of crystallinity. This means the chains are better packed and more ordered, which generally correlates with increased tensile strength and modulus. However, if the crystallinity becomes too high, the material can become less able to dissipate energy through deformation, which can lead to a decrease in toughness and make the material more brittle, as evidenced by the lower elongation at break and toughness values for the longer steam-treated samples.

In contrast, the porosity is decreased when the steam treatment is longer.[56] Porosity refers to the presence of pores or voids within the material. High porosity can act as stress concentrators within a material, which can lead to failure initiation and propagation when under tension.[57] As the steam treatment

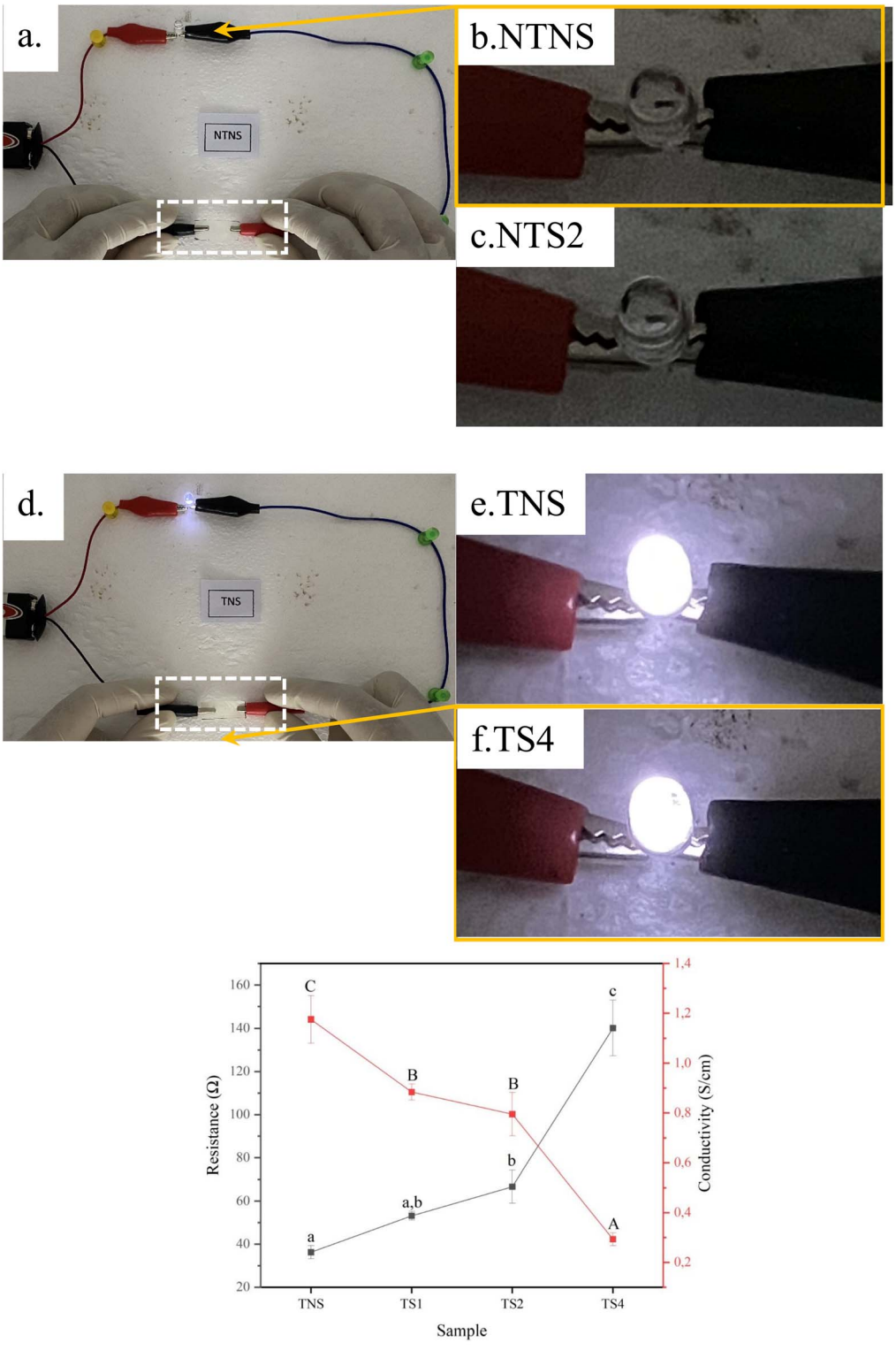

Fig. 6 Closed DC circuits (a and d). The 3 V LED connected with NTNS and NTS2 films (b and c) and TNS and TS4 films (e and f). The electrical resistance and conductivity value of the TOBC films at 50% RH (g).

duration increases, the porosity decreases, which means there are fewer defects in the material. This reduction in porosity could lead to an improvement in tensile strength since the load applied during tensile testing is distributed more uniformly across the material, without being concentrated in areas with voids.[58] However, a significant reduction in porosity could lead

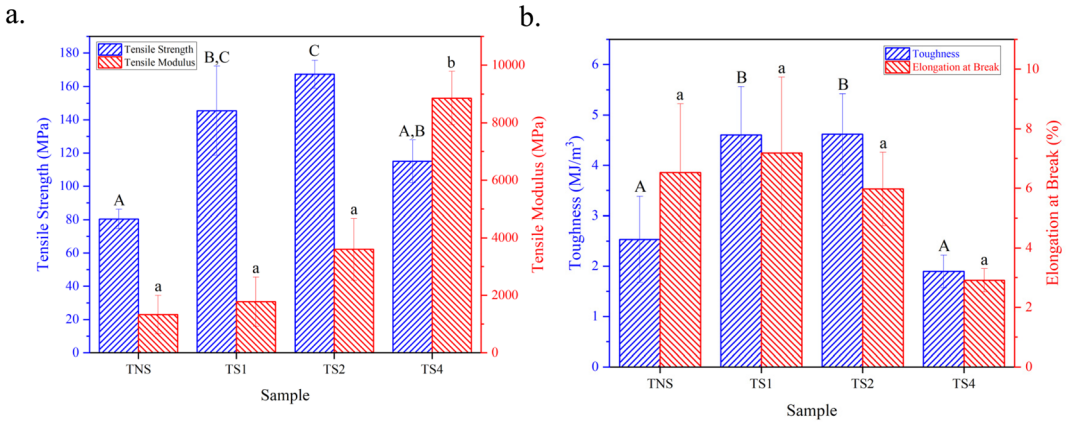

Fig. 7 Tensile strength and modulus (a), and toughness and elongation at break (b) of all films.

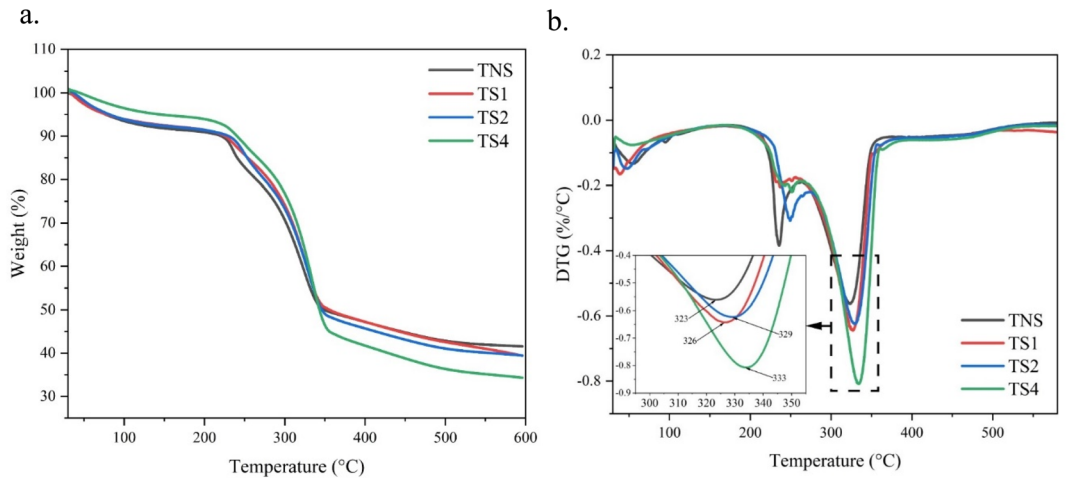

Fig. 8 Thermal properties TGA (a) and DTG (b) of all films.

to reduced toughness and elongation at break since the material has less capacity to undergo plastic deformation.

3.8 Thermal characteristics

Fig. 8 shows the thermal characteristics of samples with and without hot water vapour treatment. All samples show the type of three steps of weight loss as temperature increases. Initially, the weight loss from 50 to 170 °C was due to evaporation of absorbed water. The water evaporation level for each sample varies due to varying water content. The film without NPHWV showed the highest evaporation due to its greatest hydrophilic properties. This might be attributed to the high porous densities (Fig. 1a) and the abundance of free hydroxy groups (Fig. 2). The greatest evaporation rate of this film was 0.15% per minute, as shown in Fig. 4b. This rate reduced once the TOBC film was treated with NPHWV. As the temperature rose further, a rapid weight loss occurred due to cellulose decomposition around 260–360 °C. At temperatures over 360 °C, an additional reduction in weight was found as a result of the thermal oxidative decomposition of char.[59] The heat resistance of TOBC film is enhanced when treated with NPHWV compared to untreated TOBC film. The NPHWV treatment resulted in an increase in the maximum decomposition temperature (T_m) observed during the second weight loss, as shown in Fig. 4b and Table 1. Following a 60 minute heating period, the melting temperature (T_m) had a 2% rise, reaching 333 °C (as shown in video TS1). The T_m value (Table 1) is influenced by the crystallinity index, BC fibre density, and the number of linked hydrogen bonds between polymer chains. Therefore, a greater amount of energy is necessary to disassemble the chain-like arrangement.[60] The observed behavior aligns with the XRD pattern (Fig. 3), which exhibits more distinct peaks, and the FTIR spectrum (Fig. 2), where the C–O stretching is shifted to higher wavenumbers after undergoing NPHWV treatment. However, while longer NPHWV treatment times facilitate stronger films, this may also lead to increased brittleness, which could be a drawback. This potential weakness should be considered when optimizing treatment times, as the enhanced crystallinity and reduced water content could contribute to the material's brittleness, potentially limiting its flexibility and mechanical performance.

4. Conclusions

This study successfully demonstrated the influence of NPHWV treatment on the properties of TOBC films. The findings reveal that NPHWV treatment significantly enhances the physical, mechanical, and thermal properties of the TOBC films. The tensile strength, thermal properties, hydrophobicity, and crystallinity of the films improved with increasing duration of NPHWV treatment. Specifically, the NPHWV treatment resulted in a more hydrophobic film with a contact angle increasing from 21.47° (untreated) to 47.63° (treated for 4 h). The thermal conductivity also improved, decreasing from 0.0832 W (m K)$^{-1}$ for the untreated film to 0.0537 W (m K)$^{-1}$ for the film treated for 4 h, indicating better thermal insulation properties. Additionally, the crystallinity index (CrI) increased from 68.1% to 81.0% with 4 h of NPHWV treatment, reflecting a more ordered and compact structure.

The study highlighted the benefits of NPHWV treatment as a simple, inexpensive, and ecologically friendly method for modifying the properties of TOBC films. This method offers a sustainable alternative to more complex and chemically intensive processes traditionally used for enhancing cellulose film properties. The improved properties of NPHWV-treated TOBC films make them suitable for a wide range of applications, including functional papers, biomedical materials, electronic devices, and other advanced material applications.[21,23,25] Overall, the results of this study provide a deeper understanding of the effect of NPHWV treatment on TOBC films and open new possibilities for the utilization of bacterial cellulose in various high-performance applications. The insights gained from this research can significantly contribute to the development of more sustainable, smart, and environmentally friendly materials in the future.

Data availability

The data that support the findings of this study are available from the corresponding author upon reasonable request.

Conflicts of interest

There are no conflicts to declare.

Acknowledgements

The acknowledgment is addressed to Andalas University for supporting research funding with the project number "33/UN16.19/PT.01.03/PDD/2024."

References

1 R. Jonuarti and Suprijadi, A single tiny $Ti_n(O_2)_n$ cluster decorated an ultra-small boron nitride nanotube for hydrogen storage material: A density functional theory study, *Int. J. Hydrogen Energy*, 2022, **47**(69), 29907–29914, DOI: **10.1016/j.ijhydene.2022.06.307**.

2 R. Jonuarti, M. Yusfi and Suprijadi, Energetics and stability of hydrogen sulphide adsorption on defective carbon nanotube, *Int. J. Comput. Mater. Sci. Surf. Eng.*, 2021, **10**(1), 46–56, DOI: **10.1504/IJCMSSE.2021.116614**.

3 D. Rahmadiawan, H. Abral, S. C. Shi, T. T. Huang, R. Zainul, Ambiyar, *et al.*, Tribological Properties of Polyvinyl Alcohol/Uncaria Gambir Extract Composite as Potential Green Protective Film, *Tribol. Ind.*, 2023, **45**, 367–374, DOI: **10.24874/ti.1482.05.23.06**.

4 H. Nurdin, Waskito, A. N. Fauza, B. M. Siregar and B. K. Kenzhaliyev, The investigation of physical dan mechanical properties of Nipah-based particle board, *Teknomekanik*, 2023, **6**(2), 94–102, DOI: **10.24036/teknomekanik.v6i2.25972**.

5 S. R. P. Primandari, Mulianti, G. Sushanti, M. Gabbasa and M. M. Ba-Abbad, The effectiveness of the multi-soil-layering system in reducing pollutant parameters of crumb rubber industrial wastewater, *Teknomekanik*, 2023, **6**(2), 122–135, DOI: **10.24036/teknomekanik.v6i2.27672**.

6 H. Sehaqui, A. Liu, Q. Zhou and L. A. Berglund, Fast preparation procedure for large, flat cellulose and cellulose/inorganic nanopaper structures, *Biomacromolecules*, 2010, **11**, 2195–2198, DOI: **10.1021/bm100490s**.

7 S. C. Shi, C. F. Hsieh and D. Rahmadiawan, Enhancing mechanical properties of polylactic acid through the incorporation of cellulose nanocrystals for engineering plastic applications, *Teknomekanik*, 2024, **7**(1), 20–28, DOI: **10.24036/teknomekanik.v7i1.30072**.

8 M. Hasanin, R. M. Abdelhameed, S. Dacrory, H. Abou-Yousef and S. Kamel, Photocatalytic degradation of pesticide intermediate using green eco-friendly amino functionalized cellulose nanocomposites, *Mater. Sci. Eng. B*, 2021, **270**, 115231, DOI: **10.1016/j.mseb.2021.115231**.

9 E. Kontturi and S. Spirk, Ultrathin Films of Cellulose: A Materials Perspective, *Front. Chem.*, 2019, **7**, 1–18.

10 D. Rahmadiawan and S.-C. Shi, Enhanced Stability, Superior Anti-Corrosive, and Tribological Performance of Al2O3 Water-based Nanofluid Lubricants with Tannic Acid and Carboxymethyl Cellulose over SDBS as Surfactant, *Sci. Rep.*, 2024, **14**, 9217, DOI: **10.1038/s41598-024-59010-w**.

11 D. Rahmadiawan, S. C. Shi, Z. Fuadi, H. Abral, N. Putra, R. Irwansyah, *et al.*, Experimental investigation on stability, tribological, viscosity, and thermal conductivity of MXene/Carboxymethyl cellulose (CMC) water-based nanofluid lubricant, *J. Tribol.*, 2023, **39**, 36–50.

12 S. C. Shi, S. W. Ouyang and D. Rahmadiawan, Erythrosine–Dialdehyde Cellulose Nanocrystal Coatings for Antibacterial Paper Packaging, *Polymers*, 2024, **16**, 960, DOI: **10.3390/polym16070960**.

13 S. Wang, T. Li, C. Chen, W. Kong, S. Zhu, J. Dai, *et al.*, Transparent, Anisotropic Biofilm with Aligned Bacterial Cellulose Nanofibers, *Adv. Funct. Mater.*, 2018, **28**, 1–10, DOI: **10.1002/adfm.201707491**.

14 M. M. Abeer, M. C. I. Mohd Amin and C. Martin, A review of bacterial cellulose-based drug delivery systems: their biochemistry, current approaches and future prospects, *J.*

Pharm. Pharmacol., 2014, **66**, 1047–1061, DOI: 10.1111/jphp.12234.

15 A. Putra, R. Purnama Sari, E. Nasra, E. Yuniarti and A. Amran, Bacterial cellulose-*rambutan* leaf extract (*Nephelium lappaceum L.*) composite: preparation and characterization, *J. Phys.: Conf. Ser.*, 2021, **1876**, DOI: 10.1088/1742-6596/1876/1/012027.

16 M. Phisalaphong and N. Jatupaiboon, Biosynthesis and characterization of bacteria cellulose-chitosan film, *Carbohydr. Polym.*, 2008, **74**, 482–488, DOI: 10.1016/j.carbpol.2008.04.004.

17 E. N. Pa', N. I. A. Hamid, N. Khairuddin, K. A. Zahan, K. F. Seng, B. M. Siddique, *et al.*, Effect of different drying methods on the morphology, crystallinity, swelling ability and tensile properties of nata de coco, *Sains Malays.*, 2014, **43**, 767–773.

18 Z. Shi, Y. Zhang, G. O. Phillips and G. Yang, Utilization of bacterial cellulose in food, *Food Hydrocolloids*, 2014, **35**, 539–545, DOI: 10.1016/j.foodhyd.2013.07.012.

19 N. Soykeabkaew, C. Sian, S. Gea, T. Nishino and T. Peijs, All-cellulose nanocomposites by surface selective dissolution of bacterial cellulose, *Cellulose*, 2009, **16**, 435–444, DOI: 10.1007/s10570-009-9285-1.

20 W. Hu, S. Chen, J. Yang, Z. Li and H. Wang, Functionalized bacterial cellulose derivatives and nanocomposites, *Carbohydr. Polym.*, 2014, **101**, 1043–1060, DOI: 10.1016/j.carbpol.2013.09.102.

21 C. N. Wu and K. C. Cheng, Strong, thermal-stable, flexible, and transparent films by self-assembled TEMPO-oxidized bacterial cellulose nanofibers, *Cellulose*, 2017, **24**, 269–283, DOI: 10.1007/s10570-016-1114-8.

22 E. Lizundia, C. M. Costa, R. Alves and S. Lanceros-Méndez, Cellulose and its derivatives for lithium ion battery separators: A review on the processing methods and properties, *Carbohydr. Polym. Technol. Appl.*, 2020, **1**, 100001, DOI: 10.1016/j.carpta.2020.100001.

23 S. S. Kim, J. H. Jeon, H. Il Kim, C. D. Kee and I. K. Oh, High-Fidelity Bioelectronic Muscular Actuator Based on Graphene-Mediated and TEMPO-Oxidized Bacterial Cellulose, *Adv. Funct. Mater.*, 2015, **25**, 3560–3570, DOI: 10.1002/adfm.201500673.

24 Q. Meng and T. J. Wang, Mechanics of Strong and Tough Cellulose Nanopaper, *Appl. Mech. Rev.*, 2019, **71**, 040801, DOI: 10.1115/1.4044018.

25 C. Huang, H. Ji, Y. Yang, B. Guo, L. Luo, Z. Meng, *et al.*, TEMPO-oxidized bacterial cellulose nanofiber membranes as high-performance separators for lithium-ion batteries, *Carbohydr. Polym.*, 2020, **230**, DOI: 10.1016/j.carbpol.2019.115570.

26 P. R. Sharma, R. Joshi, S. K. Sharma and B. S. Hsiao, A Simple Approach to Prepare Carboxycellulose Nanofibers from Untreated Biomass, *Biomacromolecules*, 2017, **18**, 2333–2342, DOI: 10.1021/acs.biomac.7b00544.

27 S. S. Wong, S. Kasapis and Y. M. Tan, Bacterial and plant cellulose modification using ultrasound irradiation, *Carbohydr. Polym.*, 2009, **77**, 280–287.

28 A. Suzuki, C. Sasaki, C. Asada and Y. Nakamura, Characterization of cellulose nanofiber from steam-exploded Japanese cedar, *Bioresources*, 2017, **12**, 7628–7641, DOI: 10.15376/biores.12.4.7628-7641.

29 L. A. Jolaoso, J. Asadi, C. Duan and P. Kazempoor, A novel green hydrogen production using water-energy nexus framework, *Energy Convers. Manag.*, 2023, **276**, 116344, DOI: 10.1016/j.enconman.2022.116344.

30 F. Gao, W. Li, X. Wang, X. Fang and M. Ma, A self-sustaining pyroelectric nanogenerator driven by water vapor, *Nano Energy*, 2016, **22**, 19–26, DOI: 10.1016/j.nanoen.2016.02.011.

31 K. Huang, A. Maltais, J. Liu and Y. Wang, Food Bioscience Wood cellulose films regenerated from NaOH/urea aqueous solution and treated by hot pressing for food packaging application, *Food Biosci.*, 2022, **50**, 102177, DOI: 10.1016/j.fbio.2022.102177.

32 A. Suzuki, C. Sasaki, C. Asada and Y. Nakamura, Production of cellulose nanofibers from Aspen and Bode chopsticks using a high temperature and high pressure steam treatment combined with milling, *Carbohydr. Polym.*, 2018, **194**, 303–310, DOI: 10.1016/j.carbpol.2018.04.047.

33 J. Yin, T. Yuan, Y. Lu, K. Song, H. Li, G. Zhao, *et al.*, Effect of compression combined with steam treatment on the porosity, chemical compositon and cellulose crystalline structure of wood cell walls, *Carbohydr. Polym.*, 2017, **155**, 163–172, DOI: 10.1016/j.carbpol.2016.08.013.

34 M. Song, J. Jiang, H. Qin, X. Ren and F. Jiang, Flexible and Super Thermal Insulating Cellulose Nanofibril/Emulsion Composite Aerogel with Quasi-Closed Pores, *ACS Appl. Mater. Interfaces*, 2020, **12**, 45363–45372, DOI: 10.1021/acsami.0c14091.

35 D. Rahmadiawan, S.-C. Shi, H. Abral, M. K. Ilham, E. Sugiarti, A. N. Muslimin, *et al.*, Comparative Analysis of the Influence of Different Preparation Methods on the Properties of TEMPO-Oxidized Bacterial Cellulose Powder Films, *J. Nat. Fibers*, 2024, **21**, DOI: 10.1080/15440478.2023.2301386.

36 K. Meldawati, S. Ilyas, T. Tamrin, I. Radecka, S. Swingler, A. Gupta, *et al.*, Bioactive bacterial cellulose wound dressings for burns with collagen in situ and chitosan ex situ impregnation, *Int. J. Biol. Macromol.*, 2023, **230**, 123118, DOI: 10.1016/j.ijbiomac.2022.123118.

37 L. V. Cabañas-Romero, C. Valls, S. V. Valenzuela, M. B. Roncero, F. I. J. Pastor, P. Diaz, *et al.*, Bacterial Cellulose-Chitosan Paper with Antimicrobial and Antioxidant Activities, *Biomacromolecules*, 2020, **21**, 1568–1577.

38 D. Boon, K. Lim and H. Gong, Highly stretchable and transparent films based on cellulose, *Carbohydr. Polym.*, 2018, **201**, 446–453, DOI: 10.1016/j.carbpol.2018.08.080.

39 P. Fei, L. Liao, B. Cheng and J. Song, Quantitative analysis of cellulose acetate with a high degree of substitution by FTIR and its application, *Anal. Methods*, 2017, **9**, 6194–6201, DOI: 10.1039/c7ay02165h.

40 C. Zhang, Z. Yang, J. Shi, X. Zou, X. Zhai, X. Huang, *et al.*, Physical properties and bioactivities of chitosan/gelatin-based films loaded with tannic acid and its application on

the preservation of fresh-cut apples, *LWT*, 2021, **144**, 111223, DOI: 10.1016/j.lwt.2021.111223.

41 J. Xi, Y. Lou, Y. Chu, L. Meng, H. Wei, H. Dai, *et al.*, High-flux bacterial cellulose ultrafiltration membrane with controllable pore structure, *Colloids Surf., A*, 2023, **656**, 130428, DOI: 10.1016/j.colsurfa.2022.130428.

42 H. Abral, M. K. Chairani, M. D. Rizki, M. Mahardika, D. Handayani, E. Sugiarti, *et al.*, Characterization of compressed bacterial cellulose nanopaper film after exposure to dry and humid conditions, *J. Mater. Res. Technol.*, 2021, **11**, 896–904, DOI: 10.1016/j.jmrt.2021.01.057.

43 M. Mahardika, H. Abral, A. Kasim, S. Arief, F. Hafizulhaq and M. Asrofi, Properties of cellulose nanofiber/bengkoang starch bionanocomposites: Effect of fiber loading, *LWT–Food Sci. Technol.*, 2019, **116**, 108554.

44 S. Acharya, Y. Hu, H. Moussa and N. Abidi, Preparation and characterization of transparent cellulose films using an improved cellulose dissolution process, *J. Appl. Polym. Sci.*, 2017, **44871**, 1–12, DOI: 10.1002/app.44871.

45 M. Dilamian and B. Noroozi, A combined homogenization-high intensity ultrasonication process for individualizaion of cellulose micro-nano fibers from rice straw, *Cellulose*, 2019, **26**, 5831–5849, DOI: 10.1007/s10570-019-02469-y.

46 M. Raza, J. Mustafa, A. H. Al-marzouqi and B. Abu-jdayil, Isolation and characterization of cellulose from date palm waste using rejected brine solution, *Int. J. Thermofluids*, 2024, **21**, 100548, DOI: 10.1016/j.ijft.2023.100548.

47 W. Chen, H. Yu, Y. Liu, P. Chen, M. Zhang and Y. Hai, Individualization of cellulose nanofibers from wood using high-intensity ultrasonication combined with chemical pretreatments, *Carbohydr. Polym.*, 2011, **83**, 1804–1811.

48 H. Abral, M. M. Kadriadi, D. Handayani, E. Sugiarti and A. N. Muslimin, Characterization of disintegrated bacterial cellulose nanofibers/PVA bionanocomposites prepared via ultrasonication, *Int. J. Biol. Macromol.*, 2019, **135**, 591–599.

49 A. N. Nakagaito, M. Nogi and H. Yano, Displays from Transparent Films of Natural Nanofibers, *MRS Bull.*, 2010, **35**, 214–218, DOI: 10.1557/mrs2010.654.

50 J. Zhang, Z. Liu, Q. Kong, C. Zhang, S. Pang, L. Yue, *et al.*, Renewable and Superior Thermal-Resistant Cellulose-Based Composite Nonwoven as Lithium-Ion Battery Separator, *ACS Appl. Mater. Interfaces*, 2013, **5**, 128–134.

51 L. Kong, D. Zhang, Z. Shao, B. Han, Y. Lv, K. Gao, *et al.*, Superior effect of TEMPO-oxidized cellulose nanofibrils (TOCNs) on the performance of cellulose triacetate (CTA) ultrafiltration membrane, *Desalination*, 2014, **332**, 117–125, DOI: 10.1016/j.desal.2013.11.005.

52 J. Zhu, P. Zhu, Y. Zhu, Y. Ye, X. Sun, Y. Zhang, *et al.*, Surface charge manipulation for improved humidity sensing of TEMPO-oxidized cellulose nanofibrils, *Carbohydr. Polym.*, 2024, **335**, 122059, DOI: 10.1016/j.carbpol.2024.122059.

53 Z. Zhu, S. Fu, N. Lavoine and L. A. Lucia, Structural reconstruction strategies for the design of cellulose nanomaterials and aligned wood cellulose-based functional materials – A review, *Carbohydr. Polym.*, 2020, **247**, 116722, DOI: 10.1016/j.carbpol.2020.116722.

54 A. M. Abdel-karim, A. H. Salama and M. L. Hassan, Electrical conductivity and dielectric properties of nanofibrillated cellulose thin films from bagasse, *J. Phys. Org. Chem.*, 2018, **31**, 1–9, DOI: 10.1002/poc.3851.

55 Y. Yin, L. Berglund and L. Salmén, Effect of Steam Treatment on the Properties of Wood Cell Walls, *Biomacromolecules*, 2011, **12**, 194–202, DOI: 10.1021/bm101144m.

56 S. Tanpichai and S. Witayakran, All-cellulose composite laminates prepared from pineapple leaf fibers treated with steam explosion and alkaline treatment, *J. Reinf. Plast. Compos.*, 2017, **36**, 1146–1155, DOI: 10.1177/0731684417704923.

57 H. Sehaqui, Q. Zhou, O. Ikkala and L. A. Berglund, Strong and tough cellulose nanopaper with high specific surface area and porosity, *Biomacromolecules*, 2011, **12**, 3638–3644, DOI: 10.1021/bm2008907.

58 Ö. Keleş, N. P. Barcenas, D. H. Sprys and K. J. Bowman, Effect of Porosity on Strength Distribution of Microcrystalline Cellulose, *AAPS PharmSciTech*, 2015, **16**, 1455–1464, DOI: 10.1208/s12249-015-0325-x.

59 M. Asrofi, H. Abral, A. Kasim, A. Pratoto and M. Mahardika, Isolation of Nanocellulose from Water Hyacinth Fiber (WHF) Produced via Digester-Sonication and Its Characterization, *Fibers Polym.*, 2018, **19**, 1618–1625, DOI: 10.1007/s12221-018-7953-1.

60 A. Islam, T. Yasin and I. U. Rehman, Synthesis of hybrid polymer networks of irradiated chitosan/poly(vinyl alcohol) for biomedical applications, *Radiat. Phys. Chem.*, 2014, **96**, 115–119, DOI: 10.1016/j.radphyschem.2013.09.009.